PROCEEDINGS OF SCIENCE

Cosmic rays, gas, and dust in local clouds

Q. Remy[*†]
LUPM/CNRS/Université de Montpellier
E-mail: quentin.remy@umontpellier.fr

I. A. Grenier
AIM/CEA-IRFU/CNRS/Université Paris Diderot
E-mail: isabelle.genier@cea.fr

The recent progress in H I, CO, dust, and γ-ray observations provides excellent opportunities to probe the properties of the interstellar medium (ISM) at a resolution of a few parsecs inside nearby clouds and to search for biases in the different gas tracers. The nearby clouds in the Galactic anti-center and Chamaleon regions have been studied using jointly the γ-ray observations of the *Fermi* Large Area Telescope, and the dust optical depth inferred from *Planck* and *IRAS* observations. We have quantified the potential variations in cosmic-ray density and dust properties across the different gas phases and different clouds, and we have measured the CO-to-H_2 conversion factor, X_{CO}, in different environments. The measured interstellar γ-ray spectra support a uniform penetration of the cosmic rays with energies above a few GeV through the clouds, from the atomic envelopes to the ^{12}CO-bright cores. We find a gradual increase in dust opacity as the gas (atomic or molecular) becomes more dense which is likely caused by a chemical or structural change in the dust grains. The X_{CO} factors measured in γ rays show a decrease from diffuse to more compact molecular clouds, as expected from theory. We also mapped the gas not seen, or poorly traced, by H I, free-free, and ^{12}CO emissions, namely (i) the opaque H I and diffuse H_2 present in the Dark Neutral Medium (DNM) at the atomic-molecular transition, and (ii) the dense H_2 present where ^{12}CO lines saturate. We present these results showing how the precise modelling of the ISM we have performed helps to better trace the total gas and so improve the modelling of the diffuse Galactic γ-ray emission of interstellar origin.

7th Fermi Symposium 2017
15-20 October 2017
Garmisch-Partenkirchen, Germany

[*]Speaker.
[†]On behalf of the *Fermi*-LAT collaboration

1. Introduction

The structure, dynamics and thermodynamics of interstellar clouds is often probed with observations of the H I 21-cm line for the atomic gas (Kalberla et al. 2005, 2010; Peek et al. 2011) and of CO rotational emission lines for the molecular gas (Heyer & Dame 2015). However, measuring gas column densities in the dense media, both atomic and molecular, is hampered by the opacity of the interstellar medium (ISM) to these radiations and no efficient means exist to correct for line opacities in the absence of absorption data against background point sources. Complementary information can be gained from the sub-millimeter and infrared thermal emission of large dust grains mixed with the gas (Planck Collaboration 2014a), from the stellar reddening/extinction caused by the same dust grains, and from γ rays produced in interactions of high-energy cosmic rays (CRs) with interstellar gas nucleons (Lebrun et al. 1982). Dust grains and CRs trace all chemical and thermodynamical forms of the gas to large depths into the clouds (Planck and Fermi Collaborations 2015), but they trace only integrals of the gas column densities, $N_{\rm H}$, along sight lines, and they bear no kinematic information. To use them, we rely on critical assumptions, namely a uniform dust-to-gas mass ratio and uniform grain emission/extinction properties across a cloud and, likewise, a uniform CR flux through a cloud. Those assumptions still need to be tested in a variety of clouds and across complex phase changes, especially on consideration that dust grains and their radiation properties vary from the diffuse ISM to molecular clouds (Stepnik et al. 2003; Flagey et al. 2009; Martin et al. 2012; Roy et al. 2013; Ysard et al. 2013; Planck Collaboration 2014a,b; Planck and Fermi Collaborations 2015). One can also test the uniformity of the Local γ-ray emissivity spectrum of the gas (Casandjian 2015) in well-resolved nearby clouds to verify the smooth penetration of CRs with energies above ~1 GeV (Skilling & Strong 1976; Cesarsky & Volk 1978; Morlino & Gabici 2015).

2. Data and analyses

The results presented in the following are based on the same dust and γ-ray analyses procedures as applied to two broad regions in the anticentre (Remy et al. 2017) and in the Chamaeleon directions (Planck and Fermi Collaborations 2015) in the sky. The analysis method and multi-wavelength data used to build the γ-ray and dust models are detailed in these papers; we summarize below their main features.

In order to trace the total gas we have used the dust optical depth, τ_{353}, inferred at 353 GHz from the spectral energy distribution of the thermal emission of the large grains, which has been recorded between 353 and 3000 GHz by *Planck* and *IRAS* (Planck Collaboration 2014a). We have also used the three-dimensional stellar reddening map of Green et al. (2015) derived using both *Pan-STARRS* 1 and *2MASS* stellar data. For our analysis we have integrated this 3D $E(\mathrm{B}-\mathrm{V})$ map up to its maximal distance. Additionally we have used six years of Pass 8 photon data from the *Fermi* Large Area Telescope (LAT) between 0.4 and 100 GeV.

The γ-ray intensity, the dust optical depth, and the stellar reddening have been jointly modelled as a linear combination of H I-bright, CO-bright, and ionized gas components (plus the non-gaseous ancillary components of the γ-ray model). The coefficients of the linear combination are used to scale the dust emission/extinction and γ-ray emission of gaseous origin into gas column

density, and to probe independently the different gas phases and the different clouds separated in position-velocity. We have used 21-cm H I and 2.6-mm CO emission lines to respectively trace the atomic and CO-bright molecular hydrogen, and we have used 70-GHz free-free emission to trace the ionised gas in the anticentre region. The contribution of ionised gas in the Chamaeleon region is negligible. The only way the spatial distributions of the γ-ray intensity and of the dust optical depth can correlate is via the underlying gas structure (Grenier et al. 2005). So the joint information from dust emission and γ rays is used to reveal the gas not seen, or poorly traced, by H I, free-free, and ^{12}CO emissions, namely the opaque H I and diffuse H_2 present in the DNM, as well as the dense H_2 to be added when the ^{12}CO line emission saturates (CO_{sat}). The two templates of additional gas used in the γ-ray model are inferred from the dust model, and conversely.

3. Results and discussions

3.1 On the cosmic rays

The γ-ray emissivity of the gas in the analysed clouds has the same energy spectrum as in other clouds of the local ISM and we find no dependence of their average γ-ray emissivity with Galactocentric radius (i.e., distance from the local spiral arm), nor with height above the Galactic plane (see Fig. 1 based on Grenier et al. 2015; Remy et al. 2017, and reference therein). In the 0.4–100 GeV energy band we find no significant spectral variations except in Perseus for which we observe opposite trends for decreasing H I and increasing CO emissivities with energy. This behaviour can be attributed to the cross talk between the very compact set of H I and CO clouds in Perseus as the LAT point spread function degrades at low energies. Thus at the precision level of the current LAT observations, we find no evidence of CR exclusion or CR concentration in the clouds, up to the ^{12}CO-bright molecular regions. The *Fermi*-LAT analyses indicate that the CR population permeating the various phases of the different clouds has the same energy distribution as the average in the local ISM (Casandjian 2015), so γ rays should reliably trace most of the interstellar gas.

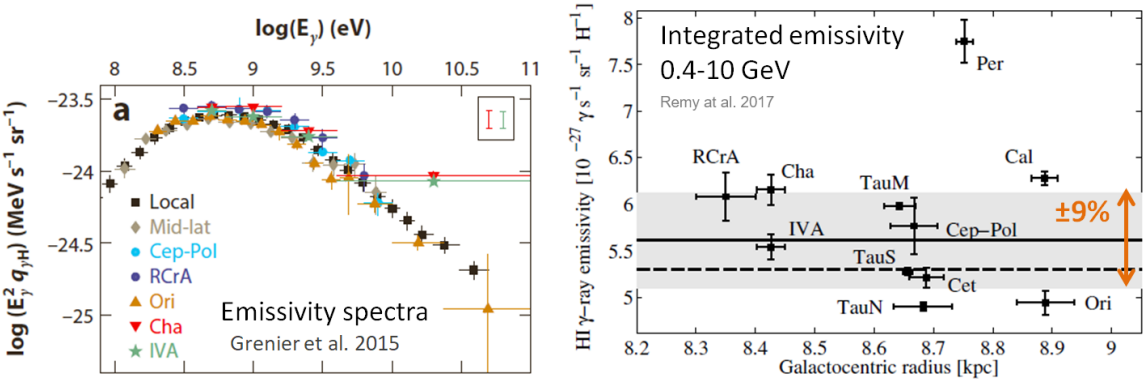

Figure 1: Left: γ-ray emissivity spectra per interstellar H atom, $q_{\gamma H}$, measured with *Fermi*-LAT data in the atomic gas of nearby clouds. Right: Distribution with Galactocentric radius of the 0.4–10 GeV emissivities measured in the atomic gas of nearby clouds for H I spin temperatures between 125 and 150 K. The solid line and grey band respectively give the average emissivity and ± 1 σ dispersion in the sample. The dashed line marks the average emissivity measured across the sky at Galactic latitudes $|b| \geq 7°$ (Casandjian 2015).

3.2 Evolution of dust properties

The dust opacity at 353 GHz, $\tau_{353}/N_{\rm H}$, in the diffuse atomic gas is about 10^{-26} cm^2. It appears to rise by a factor of three from low column densities in the atomic gas ($N_{\rm H} \sim 10^{20}$ cm^{-2}) to cold grains in molecular gas at $N_{\rm H} \gtrsim 5\times10^{21}$ cm^{-2}. The rise can reach a factor of six at very low dust temperatures below 14 K. The amplitude of the rise in the anticentre clouds is comparable to the variations observed in the Chamaeleon clouds. As the observed specific power radiated by the grains decreases in the cold molecular regions the changes cannot be attributed to a greater heating rate, but they are more likely caused by a chemical or structural change in the grains. The magnitude of the rise severely limits the use of the thermal emission of the large dust grains to trace the total gas. The linear regime is limited to $N_{\rm H} < 3\times10^{21}$ cm^{-2} in these clouds.

In contrast, we find a better correlation of the stellar reddening with the gas column density derived from γ rays (see Fig. 2). Over the whole anti-centre region the average specific reddening, $E({\rm B-V})/N_{\rm H}$, remain close to $(2.02\pm0.48)\times10^{-22}$ mag cm^2 with maximum local variations of about $\pm30\%$, at variance with the two to six-fold coincident increase seen in emission opacity as the gas column density increases. The small amplitude of the $E({\rm B-V})/N_{\rm H}$ variations with increasing $N_{\rm H}$ confirms that the large rise in opacity $\tau_{353}/N_{\rm H}$ seen toward dense CO clouds is primarily due to changes in dust emissivity. The environmental changes are qualitatively compatible with model predictions based on mantle accretion on the grains and the formation of grain aggregates (Martin et al. 2012; Köhler et al. 2015). The confirmation of large opacity variations across clouds directly impacts the gas mass estimates inferred from dust emission at sub-mm and mm wavelengths to derive star-forming efficiencies in the Galaxy and in external galaxies.

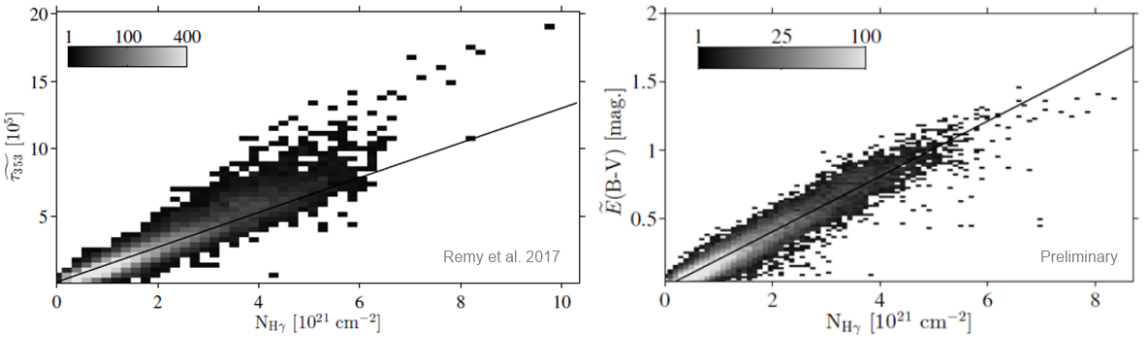

Figure 2: Left : 2D histogram of the correlation between the total gas column density measured with the 0.4–100 GeV interstellar γ rays in the anticentre clouds, and the dust optical depth at 353 GHz, convolved with the LAT response for an interstellar spectrum. The maps were sampled at a 0.375°resolution. Right : same substituting the dust optical depth, τ_{353}, by the stellar reddening, $E({\rm B-V})$.

3.3 On the dark gas

The γ-ray and dust data jointly reveal significant amounts of gas in addition to that seen in H I, free-free, and ^{12}CO emissions. The diffuse large-scale structures are associated with the DNM at the transition between the atomic and molecular phases. They gather dense atomic hydrogen and diffuse H_2 in unknown proportions, but with column densities equivalent to those found in the H I and CO emitting parts. In the molecular phase, the γ rays and dust reveal filaments of dense

gas in addition to that proportionality traced by W_{CO} where the ^{12}CO line intensities saturate. The gas column densities obtained when combining γ rays with either dust reddening or dust emission compare reasonably well in the DNM phase (H I-H_2 transition) but we find localized differences in the CO_{sat} component (dense H_2 media) due to differences in the two dust tracers (discussed above).

3.4 On the X_{CO} factors

We provide independent measurements of the X_{CO} factor from the dust and γ-ray analyses in different clouds, against the same H I and CO data. We find a better agreement between the $X_{CO} = N(H_2)/W_{CO}$ conversion factors derived with dust reddening or with γ rays than with those inferred from dust emission, especially toward clouds with large τ_{353} optical depths (see Fig. 3). The comparison confirms that the high X_{CO} values found with dust emission are biased by the significant rise in emission opacity inside molecular clouds.

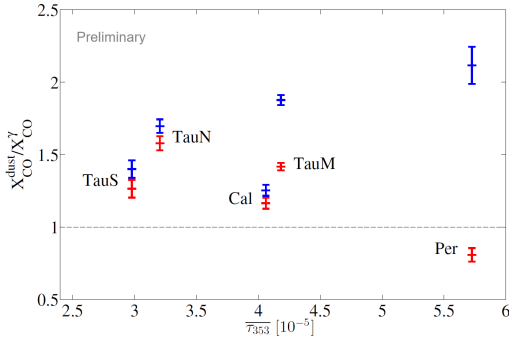

Figure 3: Comparison by ratio of the dust and γ-ray measurements of X_{CO} in the different clouds as a function of the average dust optical depth at 353 GHz in each cloud. The colours mark the use of different dust tracers : the $E(B-V)$ reddening in red, and the τ_{353} optical depth in blue.

The X_{CO} factors measured in γ rays range from $(1.04 \pm 0.05) \times 10^{20}$ cm^{-2} K^{-1} km^{-1} s in the south part of Taurus clouds to $(0.44 \pm 0.04) \times 10^{20}$ cm^{-2} K^{-1} km^{-1} s in Perseus cloud. These measurements indicate that X_{CO} values tend to decrease with the average W_{CO} intensity of a cloud, with the surface fraction subtended by the brightest CO clumps, and with the average CO line width (see Fig. 4). The more diffuse CO clouds therefore tend to have larger average X_{CO} factors. Models of the formation and photodissociation of H_2 and CO molecules predict a marked decline in X_{CO} from the diffuse envelopes of molecular clouds to their dense cores (Bell et al. 2006; Glover & Mac Low 2011; Shetty et al. 2011; Bertram et al. 2016). Hence the X_{CO} average should qualitatively vary with the surface fraction of dense regions in the cloud structure and with the CO line width, as in our data. We find a modest change by typically a factor of two in X_{CO} with cloud state, but our sample lacks a giant molecular cloud to extend the range. The amplitude of these variations already limit the precision of molecular mass estimates based on the use of CO intensities and of a mean X_{CO} conversion factor.

References

Bell, T. A., Roueff, E., Viti, S., & Williams, D. A. 2006, MNRAS, 371, 1865

Bertram, E., Glover, S. C. O., Clark, P. C., Ragan, S. E., & Klessen, R. S. 2016, MNRAS, 455, 3763

Casandjian, J.-M. 2015, ApJ, 806, 240

Cesarsky, C. J. & Volk, H. J. 1978, A&A, 70, 367

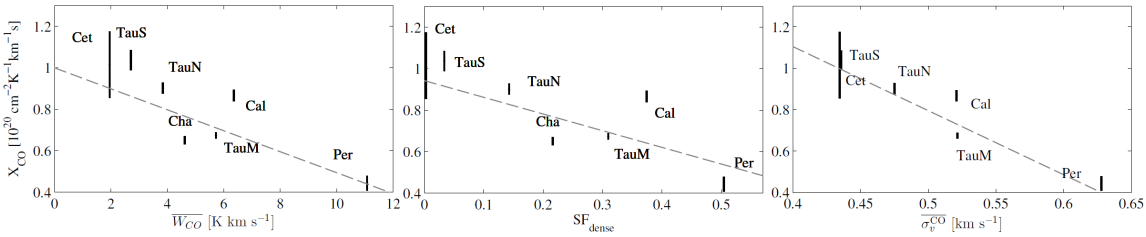

Figure 4: Evolution of the X_{CO} factor measured in γ rays as a function of the average W_{CO} intensity, $\overline{W_{CO}}$, the surface fraction of dense gas, SF_{dense}, and the average CO line width. Dashed lines give the best (χ^2) linear regressions.

Flagey, N., Noriega-Crespo, A., Boulanger, F., et al. 2009, ApJ, 701, 1450

Glover, S. C. O. & Mac Low, M.-M. 2011, MNRAS, 412, 337

Green, G. M., Schlafly, E. F., Finkbeiner, D. P., et al. 2015, ApJ, 810, 25

Grenier, I. A., Black, J. H., & Strong, A. W. 2015, ARA&A, 53, 199

Grenier, I. A., Casandjian, J.-M., & Terrier, R. 2005, Science, 307, 1292

Heyer, M. & Dame, T. M. 2015, ARA&A, 53, 583

Kalberla, P. M. W., Burton, W. B., Hartmann, D., et al. 2005, A&A, 440, 775

Kalberla, P. M. W., McClure-Griffiths, N. M., Pisano, D. J., et al. 2010, A&A, 521, A17

Köhler, M., Ysard, N., & Jones, A. P. 2015, A&A, 579, A15

Lebrun, F., Paul, J. A., Bignami, G. F., et al. 1982, A&A, 107, 390

Martin, P. G., Roy, A., Bontemps, S., et al. 2012, ApJ, 751, 28

Morlino, G. & Gabici, S. 2015, MNRAS, 451, L100

Peek, J. E. G., Heiles, C., Douglas, K. A., et al. 2011, ApJS, 194, 20

Planck and Fermi Collaborations. 2015, A&A, 582, A31

Planck Collaboration. 2014a, A&A, 571, A11

Planck Collaboration. 2014b, A&A, 566, A55

Remy, Q., Grenier, I. A., Marshall, D. J., & Casandjian, J. M. 2017, A&A, 601, A78

Roy, A., Martin, P. G., Polychroni, D., et al. 2013, ApJ, 763, 55

Shetty, R., Glover, S. C., Dullemond, C. P., & Klessen, R. S. 2011, MNRAS, 412, 1686

Skilling, J. & Strong, A. W. 1976, A&A, 53, 253

Stepnik, B., Abergel, A., Bernard, J.-P., et al. 2003, A&A, 398, 551

Ysard, N., Abergel, A., Ristorcelli, I., et al. 2013, A&A, 559, A133